# Anisotropic Thermal Diffusivity and Conductivity of YBCO(123) and YBCO(211) Mixed Crystals. I



1994 Jpn. J. Appl. Phys. 33 4965

(http://iopscience.iop.org/1347-4065/33/9R/4965)

Jpn. J. Appl. Phys. Vol. 33 (1994) pp. 4965–4970
Part 1, No. 9A, September 1994

# Anisotropic Thermal Diffusivity and Conductivity of YBCO(123) and YBCO(211) Mixed Crystals. I

Hiroyuki FUJISHIRO, Manabu IKEBE, Tomoyuki NAITO, Koshichi NOTO, Shuichi KOHAYASHI[1] and Shuji YOSHIZAWA[1]

*Department of Materials Science and Technology, Faculty of Engineering, Iwate University, 4-3-5 Ueda, Morioka 020*
[1]*Central Research Laboratory, Dowa Mining Co., Ltd., Tobukicho, Hachioji, Tokyo 192*

(Received May 31, 1994; accepted for publication July 16, 1994)

The anisotropic thermal diffusivity $\alpha$ of the highly $c$-axis-oriented Y–Ba–Cu–O bulk superconducting crystals has been measured quasi-simultaneously with the thermal conductivity $\kappa$. The estimated values of the specific heat $C$ by use of $\alpha$ and $\kappa$ values parallel and perpendicular to the $c$-direction agreed with each other. In these crystals prepared by the modified melt texture growth (MMTG) method, fine $Y_2BaCuO_5$ particles are dispersed in the $YBa_2Cu_3O_{7-x}$ superconducting matrix phase. Based on a simple model, the thermal diffusivity and the specific heat of the $YBa_2Cu_3O_{7-x}$ matrix phase are separated using independently measured data of a $Y_2BaCuO_5$ polycrystal. The influence of $Y_2BaCuO_5$ particles on the thermal properties of the mixed crystals is discussed.

KEYWORDS: Y–Ba–Cu–O superconductor, thermal diffusivity, thermal conductivity, specific heat, mixed crystal

## 1. Introduction

Y–Ba–Cu–O oxide superconductors prepared by the melt growth method are expected to be applicable to practical use owing to their high critical current density ($J_c$) and large pinning force. In these crystals, fine $Y_2BaCuO_5$ (211) phase particles are dispersed in the $YBa_2Cu_3O_{7-x}$ (123) superconducting matrix phase and are considered to act as pinning centers. The modified melt texture growth (MMTG) method is one of the melt growth methods for Y–Ba–Cu–O crystals,[1,2] and has some advantages over other methods. Firstly, since no crucibles are used for the growth, the fabrication procedure is very simple. Secondly, the grown crystals are comparatively free from impurities, because the maximum temperature of about 1100°C for the growth is lower than those of other melt growth methods, *e.g.*, quench and melt growth (QMG)[3,4] and melt texture growth (MTG).[5] The $J_c$ value of the present crystals was found to be larger than $10^4$ A/cm$^2$ at 77 K and zero field, which is comparable to those of the good crystals prepared by the QMG method.[4]

We have already reported the thermal conductivity of the $c$-axis-oriented Y–Ba–Cu–O mixed crystals prepared by MMTG.[6] The thermal conductivity was analyzed based on a proposed model for mixed crystals. As a result, the (211) phase particles decreased the conductivity of the mixed crystal in the ab-plane but only slightly influenced the conductivity along the $c$-axis.

Recently we developed a simultaneous measuring system for the thermal diffusivity $\alpha$ and the thermal conductivity $\kappa$ with an identical experimental setup.[7] This system employs a Gifford-McMahon (GM) cycle helium refrigerator as a cryostat and makes it possible to measure $\alpha$ and $\kappa$ between 10 and 200 K. Using the measured $\alpha$ and $\kappa$, the specific heat $C$ of the sample can be obtained from the relation $C=\kappa M/\rho\alpha$, where $\rho$ is the density and $M$ is the molar weight of the sample, respectively. In this paper, we study the thermal diffusivity $\alpha$ and the thermal conductivity $\kappa$ and estimate the specific heat $C$ of Y–Ba–Cu–O crystals prepared by the MMTG method. $\alpha$ and $\kappa$ have been measured both in the $ab$-plane and in the $c$-direction and the anisotropic nature of the thermal conduction is investigated. Based on the previously proposed model,[6] we also discuss the influence of the (211) phase particles on $\alpha$ and $C$.

## 2. Experimental

### 2.1 *Sample preparation*

The nominal weight ratio of the (123) phase to the (211) phase of the measured Y–Ba–Cu–O samples was 1.0:0.4. Platinum (Pt) powder was added at an amount of 0.5 wt% in order to finely disperse the (211) particles. The detailed sample preparation procedure was described elsewhere.[1,6] The sample used for the $ab$-plane measurement (#1) is $6.1\times5.9\times23.0$ mm$^3$ with the $6.1\times23.0$ mm$^2$ plane perpendicular to the $c$-axis. The sample for the $c$-direction measurement (#2) was $2.8\times3.9\times12.0$ mm$^3$ with the 12.0-mm length parallel to the $c$-axis. The crystal axes of the samples were determined by an X-ray diffraction method. The (211) polycrystals were prepared by a solid state reaction method. Mixed powder of $Y_2O_3$, $BaCO_3$ and CuO with a mole ratio of 1:1:1 was calcined at 950°C for 15 h in air. After pulverizing the calcined materials, they were pressed into a pellet and sintered at 990°C for 24 h in air.

### 2.2 *Measurement*

Figure 1 shows a schematic diagram of the experimental setup for the thermal diffusivity and conductivity measurement. The vacuum chamber was evacuated to below $10^{-5}$ Torr by an oil diffusion pump. One end of the sample was soldered to the cold head of the GM refrigerator and a small metal film chip resistor was adhered to the other end of the sample as a heater by GE7031 varnish. Au(Fe)-chromel thermocouples (73 $\mu$m in diameter) were used differentially to monitor the temperatures $T_1$ and $T_2$ at the positions $P_1$ and $P_2$. Digital voltmeters (DVMs), current sources, a personal computer, and other equipment were connected using GP-IB and RS-232C interface bus lines. This automatic measuring system of $\alpha$ and $\kappa$ was operated in the temperature range from 10 to 200 K.[7–10] The thermal con-

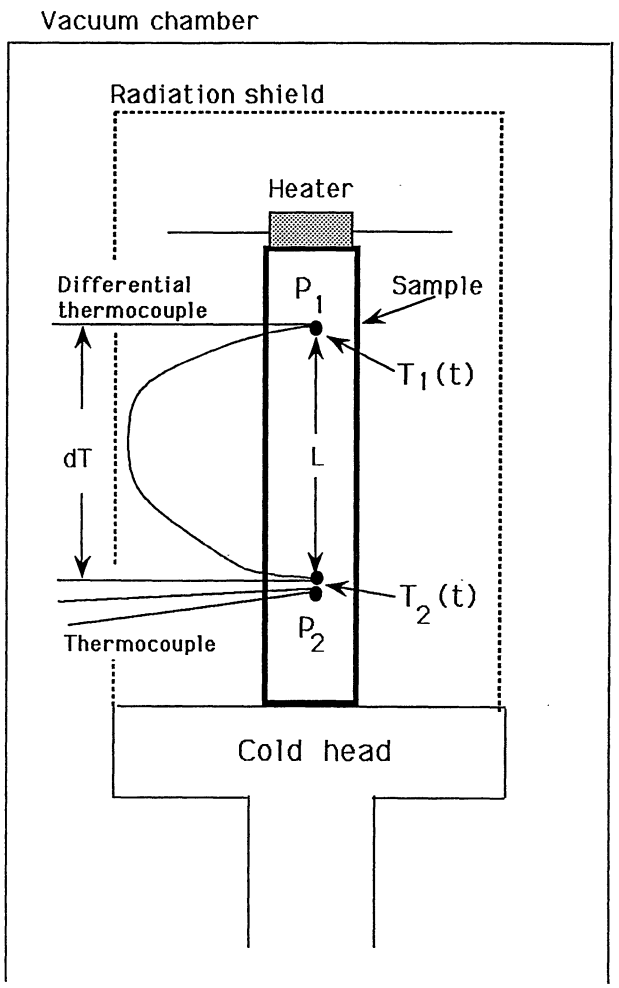


Fig. 1. Schematic diagram of the sample configuration of the thermal diffusivity and conductivity measurement system using a GM cycle helium refrigerator.

ductivity was measured by a steady-state heat flow method and the thermal diffusivity was measured by an arbitrary heating method, which is one of the non-steady-state heat flow methods. The detailed procedure used to determine the diffusivity is explained in the following subsection.

2.3 *Determination of the thermal diffusivity* $\alpha$

When a heat pulse is applied from a heater to a long sample, the time variation of temperature $T(x, t)$ at a position $x$ is described by the following one-dimensional diffusion equation,

$$\frac{\partial T(x, t)}{\partial t} = \alpha \frac{\partial^2 T(x, t)}{\partial x^2}, \tag{1}$$

where $\alpha$ is the diffusivity. This equation can be numerically solved by the Crank-Nicolson implicit method[11] by converting it into approximate difference equations. After introducing the boundary conditions, we obtain n-dimensional linear equations, which are solved by the Gaussian elimination method. In the measurement, the temperature changes $T_1(t)$ and $T_2(t)$ at the two measuring points $P_1$ and $P_2$ were recorded 3.1 times a second for 100–150 s. The temperature change $T_1(t)$ was used for the boundary condition of the diffusion equation in order to calculate the temperature change of $T_2(t)$ at the point of $P_2$ for an arbitrary $\alpha$. This method has an advantage that $T_2(t)$ can be calculated precisely even if the shape of the heat impulse is disturbed when it passes through the sample surface. In order to determine the optimum $\alpha$ values systematically, the maximum values of the experimentally observed $T_2(t)$ curve and the calculated $T_2'(t)$ one were reduced to 1 and eighty points in the range from 0.1 to 0.9 of the rising part of $T_2(t)$ were sampled to obtain the minimum squared time error $\langle \Delta t^2 \rangle$ between the observed and calculated curves. The method was confirmed to have $\pm 1.5\%$ precision and $\pm 5\%$ accuracy for various $\alpha$ values.[7]

## 3. Experimental Results

Figure 2 shows the temperature dependences of the $ab$-plane thermal conductivity $\kappa_{ab}$ and the $c$-axis thermal conductivity $\kappa_c$. The transition temperature $T_c$ of these two MMTG samples (#1, #2) was determined to be 90 K from the resistive measurements (see Fig. 1 in the following Paper II[12]). $\kappa_{ab}$ increases slightly from 200 K to $T_c$ with decreasing temperature, and shows a remarkable upturn below $T_c$. The maximum of $\kappa_{ab}$ occurs at around 50 K and then $\kappa_{ab}$ decreases with further decrease of temperature. $\kappa_c$ is almost constant above about 100 K, increases slightly below about 100 K with decreasing temperature and then decreases sharply below $\approx 50$ K. The observed anisotropy ratio $\kappa_{ab}/\kappa_c$ is about 4.0 in the normal state.

Figure 3 shows the temperature dependences of the $ab$-plane thermal diffusivity $\alpha_{ab}$ and $c$-axis thermal diffusivity $\alpha_c$. In the normal state, $\alpha_{ab}(T)$ and $\alpha_c(T)$ increase slightly with decreasing temperature. Below $T_c$, the gradient of $\alpha_{ab}(T)$ changes and increases more and more rapidly with decreasing temperature. For the $c$-axis thermal diffusivity, the gradient change of $\alpha_c(T)$ below $T_c$ is hardly discernible. The diffusivity shows anisotropy similar to the thermal conductivity. The observed anisotropy ratio $\alpha_{ab}/\alpha_c$ is also about 4.0 in the normal state. The observed characteristics of the in-plane thermal diffusivity are in accord with those

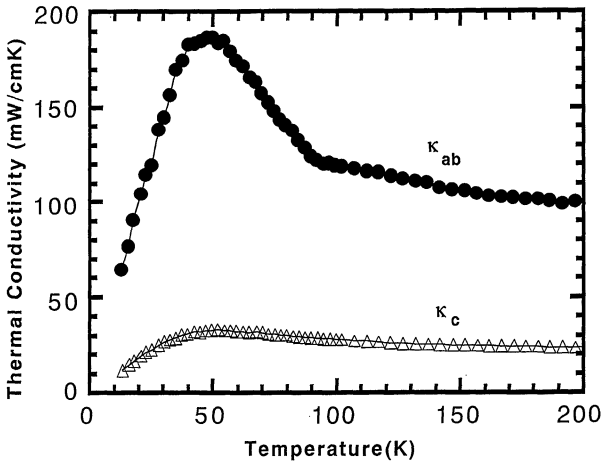


Fig. 2. Temperature dependence of the thermal conductivity of the MMTG samples in the $ab$-plane ($\kappa_{ab}$, sample #1) and along the $c$-axis ($\kappa_c$, sample #2).

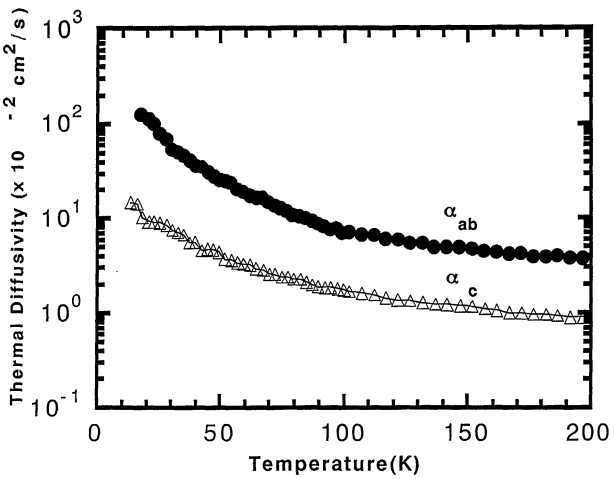


Fig. 3. Temperature dependence of the thermal diffusivity of the MMTG samples in the *ab*-plane ($\alpha_{ab}$, sample #1) and along the *c*-axis ($\alpha_c$, sample #2).

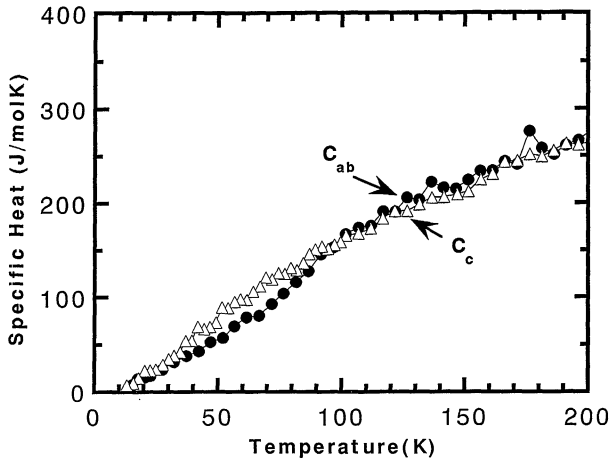


Fig. 4. Temperature dependence of the estimated specific heat. $C_{ab}$ is calculated based on $\kappa_{ab}$ and $\alpha_{ab}$ (sample #1) and $C_c$ is based on $\kappa_c$ and $\alpha_c$ (sample #2).

reported for the other oxide superconductors.[13-16]

Figure 4 shows the specific heat $C$ (J/molK) of these crystals calculated using the relation $C=\kappa M/\rho\alpha$. In Fig. 4, $C_{ab}$ is the specific heat calculated using $\kappa_{ab}$ and $\alpha_{ab}$, and $C_c$ is calculated using $\kappa_c$ and $\alpha_c$. In the calculation, the measured value of $\rho=5.94$ g/cm$^3$ and average molar weight $M_{\mathrm{MMTG}}=589.8$ g were used, because the present crystals are composed of the (123) phase ($M_{123}=666.0$ g) and the (211) phase ($M_{211}=458.6$ g) with the molar ratio of (123):(211)=(1.0/666.0):(0.4/458.6). $C_{ab}$ and $C_c$ are in good agreement over the entire temperature range below 200 K. This agreement supports the reliability of the present measurements of $\alpha$ and $\kappa$.

In order to investigate the influence of the (211) phase particles on the values of $\alpha$, $\kappa$ and $C$ of the MMTG sample, the thermal diffusivity $\alpha^{211}$ and conductivity $\kappa^{211}$ of the (211) polycrystal were also measured and the specific heat $C^{211}$ was estimated. Figure 5 shows the temperature dependences of $\alpha^{211}$ and $\kappa^{211}$. Since the (211) polycrystal is an insulator, the heat conduction is considered to be due to phonons. $\kappa^{211}(T)$ increases slightly with decreasing temperature, shows a maximum at about 50 K, and then decreases with further decrease of temperature. $\alpha^{211}(T)$ also increases with decreasing temperature and increases very rapidly below 40 K. Figure 6 shows the specific heat of the (211) phase $C^{211}$, calculated using the values of $\kappa^{211}$, $\alpha^{211}$, $M_{211}$(=458.6 g) and $\rho_{211}$(=3.1 g/cm$^3$ which was the measured value).

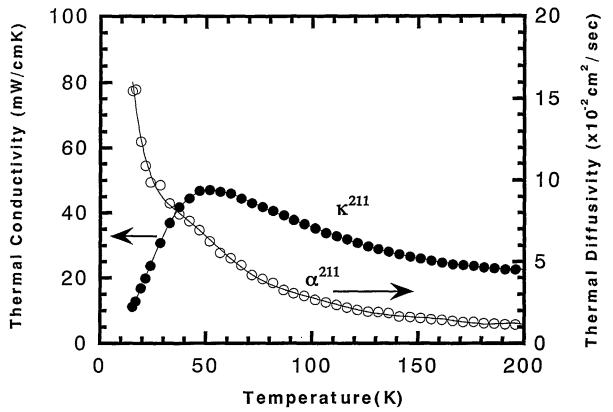


Fig. 5. Temperature dependences of the thermal conductivity ($\kappa^{211}$) and thermal diffusivity ($\alpha^{211}$) of the sintered $Y_2BaCuO_5$ polycrystal.

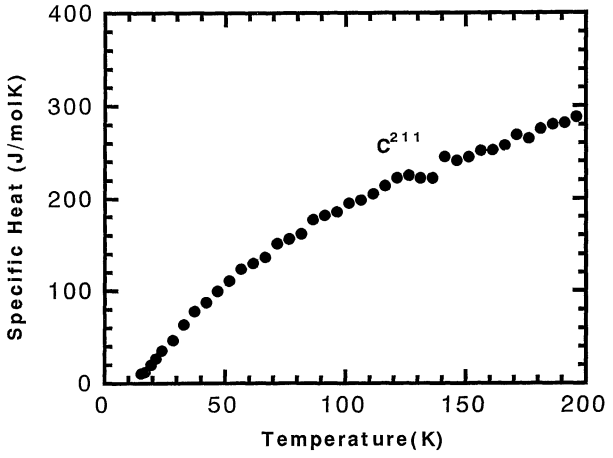


Fig. 6. Calculated specific heat ($C^{211}$) of the sintered (211) polycrystal using $\kappa^{211}$ and $\alpha^{211}$ shown in Fig. 5.

## 4. Discussion

### 4.1 *Influence of the (211) phase particles on the specific heat*

The specific heat of MMTG crystal $C_{\mathrm{MMTG}}$, is represented using $C^{123}$ and $C^{211}$ as

$$C_{\mathrm{MMTG}}=(1-X)C^{123}+XC^{211}, \qquad (2)$$

where $X$(=(0.4/458.6)/(1.0/666.0+0.4/458.6)=0.366) is the molar ratio of the (211) phase in the present crystal. Using this relation and the measured $C_{\mathrm{MMTG}}$ and $C^{211}$ values, the specific heat of the (123) matrix phase $C^{123}$ was estimated. Figure 7 shows the estimated specific heat. In this figure, $C_{ab}^{123}$ and $C_c^{123}$ are the specific heat calculated from the data of samples #1 and

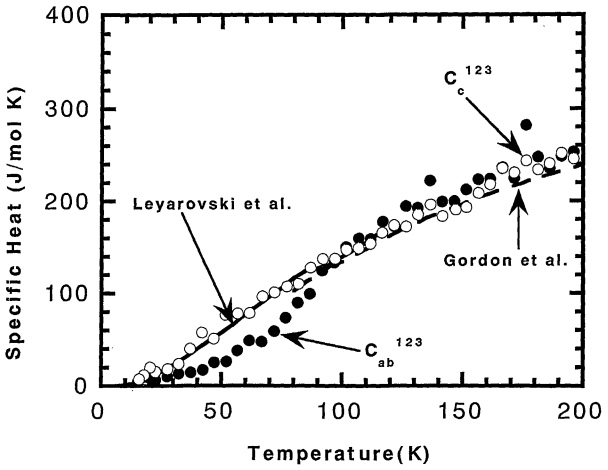


Fig. 7. Temperature dependence of the specific heat of the (123) matrix phase in the MMTG mixed crystals. $C_{ab}^{123}$ and $C_c^{123}$ show the specific heat calculated using the data in the $ab$-plane (sample #1) and along the $c$-axis (sample #2), respectively. Reported data are also shown.

#2, respectively. The specific heat data of the (123) phase reported by Leyarovski *et al.*[17] and Gordon *et al.*[18] are also shown. The reported data measured by an adiabatic calorimeter[17] and a conventional heat pulse method[18] are only slightly below $C_{ab}^{123}$ and $C_c^{123}$.

### 4.2 *Influence of the (211) phase particles on the thermal conductivity*

In the MMTG crystals, a number of (211) phase fine particles are dispersed in the (123) matrix, as schematically shown in Fig. 8(a). In the previous study for the thermal conductivity of MMTG crystals,[6] we proposed a simple model for the heat conduction of the mixed crystals. In this model, all the (211) particles in the cubic sample with a side length of $a_0$ are concentrated into a small cubic (211) polycrystal embedded into the (123) matrix phase, as shown in Fig. 8(b). Thus we approximate the contribution of the (211) particles to the heat path by the small polycrystal cube. Because the ideal densities of the (211) and (123) phases are almost the same, the weight ratio can be regarded as the volume ratio of the (211) and (123) phases. Therefore, if the (211) volume ratio is $x_0$ ($=0.286$), the side length of the (211) polycrystal cube is assumed to be $\sqrt[3]{x_0}a_0$. The thermal resistance W of the specimen is given by an equivalent circuit schematically shown in Fig. 8(c),

$$W=\frac{1}{a_0\kappa}=W_{123}+\frac{W'_{123}W_{211}}{W'_{123}+W_{211}}, \tag{3}$$

where $W_{123}=(1-\sqrt[3]{x_0})/[a_0\kappa^{123}]$, $W'_{123}=\sqrt[3]{x_0}/[a_0(1-\sqrt[3]{x_0^2})\kappa^{123}]$ and $W_{211}=1/[a_0\sqrt[3]{x_0}\kappa^{211}]$. We can deduce the conductivity value $\kappa^{123}$ of the (123) phase in the present mixed crystals using $\kappa^{211}$ shown in Fig. 5.

Figure 9 shows the calculated $\kappa_{ab}^{123}$ and $\kappa_c^{123}$ in which the measured $\kappa_{ab}$ and $\kappa_c$ are also shown. For sample #1, the calculated $ab$-plane thermal conductivity $\kappa_{ab}^{123}$ is fairly large and the measured $\kappa_{ab}$ is appreciably reduced by the dispersed particles of the low thermally conductive (211) phase. On the other hand, the calculated $c$-axis

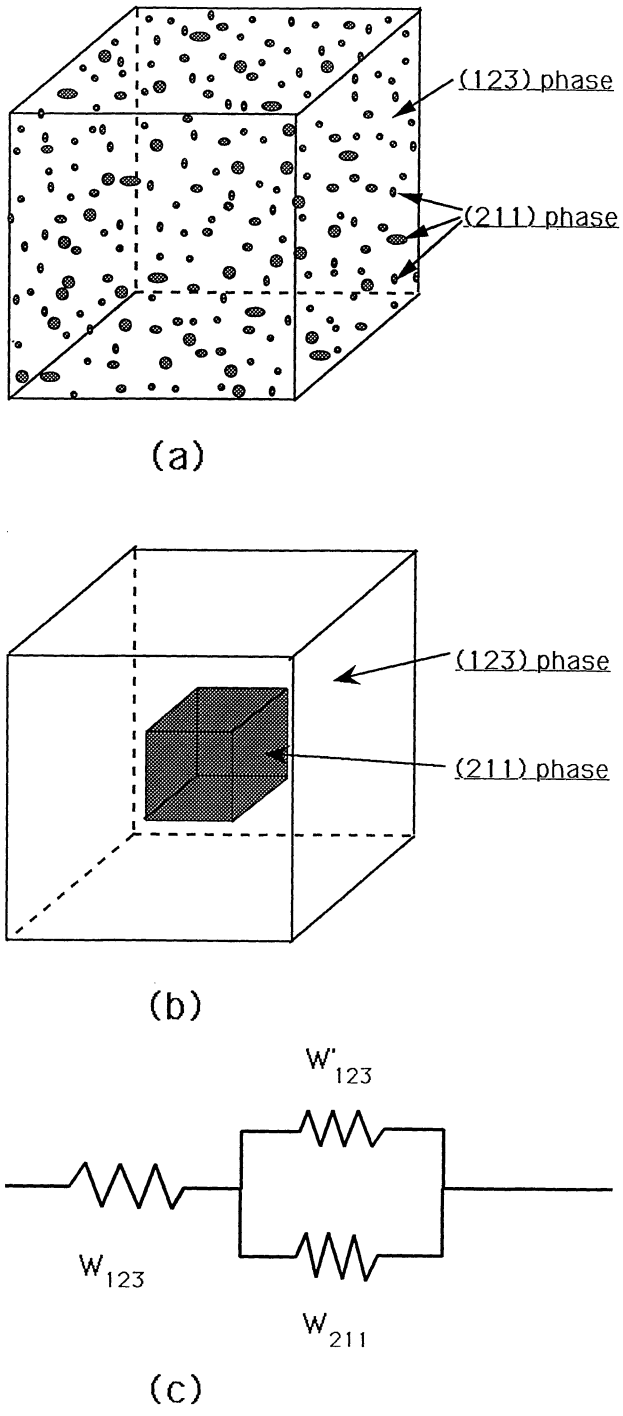


Fig. 8. Schematic presentation of the present model: (a) mixed crystal in which (211) phase particles are finely dispersed; (b) a model structure to estimate the thermal resistance W; (c) an equivalent circuit to calculate the thermal resistance W.

conductivity $\kappa_c^{123}$ for sample #2 is slightly smaller than the measured $\kappa_c$ because of the somewhat higher thermal conductivity of the (211) phase in comparison with $\kappa_c$. Accordingly, the anisotropy ratio $\kappa_{ab}^{123}/\kappa_c^{123}$ is estimated to be about 6.6 above $T_c$ for the matrix (123) phase.

### 4.3 *Estimation of $\alpha_{ab}^{123}$ and $\alpha_c^{123}$*

In this subsection, we estimate the influence of the (211) phase particles on the thermal diffusivity. We can

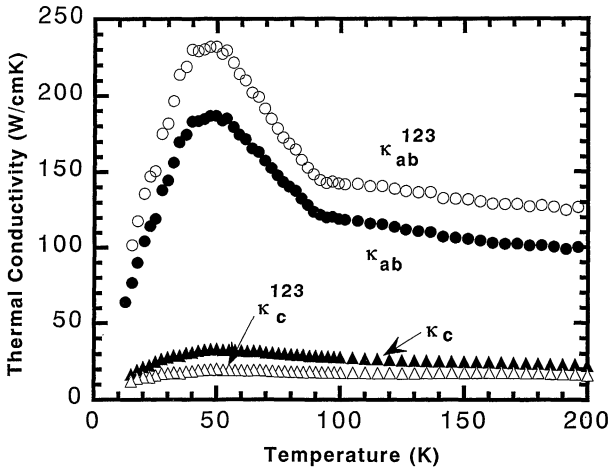


Fig. 9. The results of the model calculation for the *ab*-plane thermal conductivity $\kappa_{ab}^{123}$ (○) and the *c*-axis conductivity $\kappa_c^{123}$ (△) are shown together with the measured $\kappa_{ab}$ (●) and $\kappa_c$ (▲).

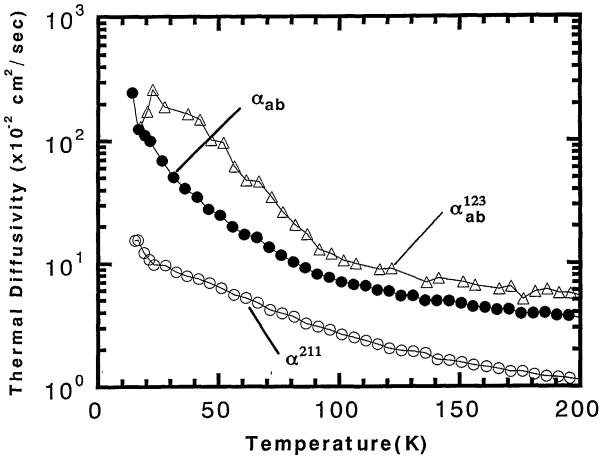


Fig. 10. Estimated *ab*-plane thermal diffusivity $\alpha_{ab}^{123}$ of the (123) matrix phase in the MMTG sample. Measured thermal diffusivity data of sample #1 $\alpha_{ab}$ and the (211) polycrystal $\alpha^{211}$ are also shown for comparison.

obtain the *ab*-plane and *c*-axis thermal diffusivities of the (123) matrix phase using the relation $\alpha^{123}=\kappa^{123}M_{123}/\rho_{123}C^{123}$. For the estimation using this relation, the specific heat shown in Fig. 7 was used for $C^{123}$, and the thermal conductivity of the (123) matrix phase $\kappa^{123}$ in Fig. 9 was used for $\kappa^{123}$.

Figure 10 shows the temperature dependence of the *ab*-plane thermal diffusivity of the (123) matrix phase $\alpha_{ab}^{123}$. In this figure, the measured thermal diffusivity $\alpha_{ab}$ and that of the (211) polycrystal $\alpha^{211}$ are also shown. The measured $\alpha_{ab}$ was about 40% smaller than $\alpha_{ab}^{123}$ at 200 K because $\alpha^{211}$ is smaller than $\alpha_{ab}$. Figure 11 shows the temperature dependence of *c*-axis thermal diffusivity of the (123) matrix phase $\alpha_c^{123}$. In this figure, the measured thermal diffusivity $\alpha_c$ and that of the (211) phase $\alpha^{211}$ are also shown. Because of the higher thermal diffusivity of the (211) phase than that of $\alpha_c$, the measured $\alpha_c$ was about 15% larger than $\alpha_c^{123}$ at 200 K. The existence of the (211) phase somewhat enhances the *c*-axis thermal diffusivity. The anisotropy ratio of the (123) matrix phase $\alpha_{ab}^{123}/\alpha_c^{123}$ was 6.7 at 200 K which was larger than the measured anisotropic ratio of the MMTG sample $\alpha_{ab}/\alpha_c(=4.0)$. In this way, it is shown that the (211) phase particles reduce the thermal diffusivity in the *ab*-plane but enhance the diffusivity along the *c*-axis in the MMTG crystals.

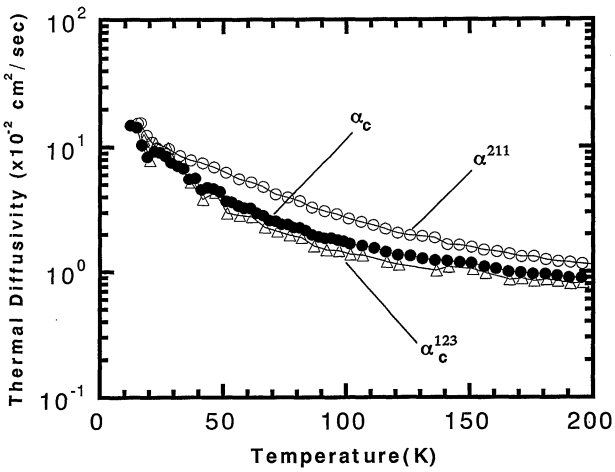


Fig. 11. Estimated *c*-axis thermal diffusivity $\alpha_c^{123}$ of the (123) matrix phase in the MMTG sample. Measured thermal diffusivity data of sample #2 $\alpha_c$ and the (211) polycrystal $\alpha^{211}$ are also shown for comparison.

## 5. Conclusions

The anisotropic thermal diffusivity $\alpha$ of YBCO(123) and YBCO(211) mixed crystals prepared by the MMTG method was measured quasi-simultaneously with the thermal conductivity $\kappa$. The values of the estimated specific heat based on the data of the diffusivity and conductivity parallel and perpendicular to the crystalline *c*-axis agreed with each other. Based on a simple model, the diffusivity and conductivity of the (123) matrix phase were estimated using the data of the (211) polycrystal. The influence of the (211) particles on the thermal properties was discussed. As a result, it was found that the (211) phase reduces the thermal diffusivity and conductivity in the *ab*-plane, but somewhat enhances them along the *c*-axis.

## Acknowledgments

The authors wish to thank Miss T. Nakagawa of Iwate University for her assistance in the thermal diffusivity and the specific heat analyses and Dr. M. Matsukawa of Iwate University for valuable discussion.

1) S. Kohayashi, Y. Ishikawa, S. Yoshizawa and H. Kojima: *Proc. Int. Superconducting Symp. (ISS) '92* (Springer-Verlag, Tokyo, 1993) p. 795.
2) K. Tenya, H. Miyajima, Y. Ishikawa, S. Kohayashi and S. Yoshizawa: J. Mag. Soc. Jpn. **16** (1992) 467.
3) M. Murakami, M. Morita, K. Doi and M. Miyamoto: Jpn. J. Appl. Phys. **28** (1988) 1189.
4) K. Sawano, M. Miura, M. Tanaka, K. Kimura, S. Takebayashi, M. Kimura and K. Miyamoto: *Proc. Int. Superconducting Symp. (ISS) '90* (Springer-Verlag, Tokyo, 1991) p. 715.

5) S. Jin, T. H. Tiefel, R. C. Sherwood and R. B. Dover: Phys. Rev. B **37** (1988) 7850.
6) M. Ikebe, H. Fujishiro, T. Naito, K. Noto, S. Kohayashi and S. Yoshizawa: Cryogenics **34** (1994) 57.
7) H. Fujishiro, T. Naito, M. Ikebe and K. Noto: Cryo. Eng. **28** (1993) 533 [in Japanese].
8) H. Fujishiro, M. Ikebe, T. Naito, M. Matsukawa and K. Noto: Cryo. Eng. **28** (1993) 582 [in Japanese].
9) M. Ikebe, H. Fujishiro, T. Naito and K. Noto: J. Phys. Soc. Jpn. **63** (1994) 3107.
10) N. Hobara, M. Matsukawa, N. Matsuura, H. Fujishiro and K. Noto: Cryo. Eng. **28** (1993) 688 [in Japanese].
11) J. Crank: *The Mathematics of Diffusion* (Clarendon Press, London, 1975) p. 144.
12) M. Ikebe, H. Fujishiro, T. Naito, M. Matsukawa and K. Noto: to be publishied in Jpn. J. Appl. Phys.
13) T. Higashi, M. Onuki, S. Ishii, H. Kubota and T. Fujiyoshi: Physica C **185–189** (1991) 1357.
14) J. Issac, J. Philip and B. K. Chaudhuri: Paramana-J. Phys. **32** (1989) L167.
15) S. B. Peralta, Z. H. Chen and A. Mandelis: Appl. Phys. A **52** (1991) 289.
16) M. Marinelli, F. Murtas, M. G. Mecozzi, U. Zammit, R. Pizzoferrato, F. Scudieri, S. Martellucci and M. Marinelli: Appl. Phys. A **51** (1990) 387.
17) E. Leyarovski, N. Leyarovska, C. H. R. Popov and M. Kirov: Physica C **153–155** (1988) 1022.
18) J. E. Gordon, R. A. Fisher, S. Kim and N. E. Phillips: Physica C **162–164** (1989) 484.